

Potential for measuring the $H^\pm W^\mp Z^0$ vertex from WZ fusion at the Large Hadron Collider

Eri Asakawa,^{1,*} Shinya Kanemura,^{2,†} and Junichi Kanzaki^{3,‡}

¹*Theory Group, KEK,*

Tsukuba, Ibaraki 305-0801, Japan

²*Department of Physics, University of Toyama,*

3190 Gofuku, Toyama 930-8555, Japan

³*Institute of Particle and Nuclear Studies, KEK,*

Tsukuba, Ibaraki 305-0801, Japan

Abstract

We investigate the possibility of measuring the $H^\pm W^\mp Z^0$ vertex from the single H^\pm production process via WZ fusion at the CERN Large Hadron Collider (LHC). This vertex strongly depends on the structure of the Higgs sector in various new physics scenarios, so that its measurement can be useful to distinguish the models. A signal and background simulation under the expected detector performance at the LHC is done for the processes of $pp \rightarrow W^\pm Z^0 X \rightarrow H^\pm X \rightarrow tbX$ and $pp \rightarrow W^\pm Z^0 X \rightarrow H^\pm X \rightarrow W^\pm Z^0 X$, and the required magnitudes of the $H^\pm W^\mp Z^0$ vertex for observation are evaluated. It is found that although the loop induced $H^\pm W^\pm Z^0$ vertex in multi-Higgs doublet models cannot be measurable, the latter process can be useful to test the model with a real and a complex triplets.

PACS numbers: 12.60.Fr, 14.80.Cp

Keywords: Higgs, LHC, Beyond the Standard Model

*Electronic address: eri@post.kek.jp

†Electronic address: kanemu@sci.u-toyama.ac.jp

‡Electronic address: Junichi.Kanzaki@cern.ch

I. INTRODUCTION

The idea of spontaneous breaking of the electroweak gauge symmetry will soon be tested directly at the CERN Large Hadron Collider (LHC) [1]. There, it is expected that a Higgs boson of the standard model (SM) can be detected in a wide range of the mass, which is the last unknown parameter of the model. On the other hand, it is possible that the structure of the Higgs sector takes a non-minimal form with additional isospin-singlets, doublets, triplets etc. In fact, there is a variety of new physics scenarios which deduce extended Higgs sectors in the low energy effective theory.

In extended Higgs models, additional scalar bosons like charged and CP-odd Higgs bosons are predicted. There are plenty of studies on production mechanisms of such extra Higgs bosons. At the LHC, charged Higgs bosons H^\pm in two Higgs doublet models (2HDMs), including the minimal supersymmetric standard model (MSSM), are produced via $gg \rightarrow H^\pm tb$ (or $gb \rightarrow H^\pm t$) [2], $gg(q\bar{q}) \rightarrow H^+ H^-$ [3] and $gg(q\bar{q}) \rightarrow H^\pm W^\mp$ [4] when $m_{H^\pm} \gtrsim m_t$, while they are produced via $t \rightarrow bH^\pm$ for $m_{H^\pm} \lesssim m_t - m_b$ [1, 5]. These processes are primarily important for discovery of charged Higgs bosons in such models. On the other hand, if the Higgs sector includes greater multiplets than doublets, the production and the decay of the singly-charged Higgs bosons can be completely different from those in the 2HDMs. Therefore, it is valuable to study more observables which can be measured at future experiments in order to determine the Higgs sector.

For the structure of the Higgs sector, the current electroweak data provide important hints. In particular, all the Higgs models must respect the experimental fact that the electroweak rho parameter (ρ) is very close to unity. It is well known that the tree-level prediction of $\rho = 1$ is a common feature of Higgs models with only doublets (and singlets) [6]. On the contrary, the rho parameter data give a strong constraint on the models which additionally include triplets or greater representations of the isospin $SU(2)$ gauge symmetry, because in these cases the predicted rho parameter is generally not unity already at the tree level [7]. There are two simple possibilities to satisfy this constraint in such models. First, these multiplets but doublets do not contribute to the electroweak spontaneous symmetry breaking much, and their vacuum expectation values are sufficiently small as compared to

those of doublets¹. Second, we can consider models arranging the custodial $SU(2)$ symmetry among these additional multiplets, so that the models then naturally impose $\rho = 1$ at the tree level [12, 13, 14, 15].

After the discovery of extra Higgs bosons, the Higgs sector must be explored by measuring their masses and various coupling constants etc. For the exploration of the global symmetry structure of the Higgs sector, the coupling of singly-charged Higgs bosons with the weak gauge bosons, $H^\pm W^\mp Z^0$, is of particular importance [6, 16, 17, 18, 19, 20]. It can appear at the tree level in models with scalar triplets, while it is induced at the loop level in multi scalar doublet models. In Ref. [20], the new physics predictions to the $H^\pm W^\mp Z^0$ are summarized and possible size of the signal cross section in each model is evaluated. The vertex is expressed by

$$i\Gamma_{H^\pm W^\mp Z}(p_W, p_Z; \lambda_W, \lambda_Z) = igm_W V_{\mu\nu} \epsilon_W^{*\mu}(p_W, \lambda_W) \epsilon_Z^{*\nu}(p_Z, \lambda_Z), \quad (1)$$

where g is the weak gauge coupling, m_W is the mass of the weak boson W^\pm , and $\epsilon_V^{*\mu}(p_V, \lambda_V)$ ($V = W$ and Z) are polarization vectors for the outgoing weak gauge bosons with the momentum p_V and the helicity λ_V . Here, $V_{\mu\nu}$ is decomposed in terms of three form factors as

$$V_{\mu\nu} = F g_{\mu\nu} + \frac{G}{m_W^2} p_{Z\mu} p_{W\nu} + \frac{H}{m_W^2} \epsilon_{\mu\nu\rho\sigma} p_Z^\rho p_W^\sigma, \quad (2)$$

where the antisymmetric tensor $\epsilon_{\mu\nu\rho\sigma}$ is defined so as to satisfy $\epsilon_{0123} = -1$. The values of F , G and H depend on the detail of the model. The leading contribution is well described by F , and its magnitude is directly related to the structure of the extended Higgs sector under global symmetries[6, 7].

In this paper, we consider testing the $H^\pm W^\mp Z^0$ coupling via the single charged Higgs boson production in the WZ fusion process at the LHC. In general, neutral Higgs production processes via vector boson fusion (VBF) have an advantage over the other production processes, because the signal can be completely reconstructed and produced jets are suppressed in the central region due to a lack of color flow between the initial state quarks [1, 21, 22, 23, 24]. The same benefit can also be applied to H^\pm production

¹ This type of models includes the Left-Right symmetric model [8], the Littlest Higgs model [9, 10] and some extra dimension models [11] which predict an additional complex triplet.

from WZ fusion. A signal and background simulation under the expected detector performance at the LHC is performed for the processes of $pp \rightarrow W^\pm Z^0 X \rightarrow H^\pm X \rightarrow tbX$ and $pp \rightarrow W^\pm Z^0 X \rightarrow H^\pm X \rightarrow W^\pm Z^0 X$. We estimate the minimum value of the form factor $|F|^2$ above which the signal significance can be substantial for a possibility of detection at the LHC. We then discuss which new physics models can be tested via these processes.

II. POSSIBLE VALUES OF THE $H^\pm W^\mp Z^0$ VERTEX IN SEVERAL MODELS

We here shortly summarize typical values of the form factor F in several new physics models[20]; i.e., 2HDMs (including the MSSM)[16, 17, 18, 19, 25, 26, 27, 28], the Littlest Higgs model[9, 10], and the model with a real and a complex triplet fields[12, 13, 14].

In the 2HDM², there are two sources to enhance the loop-induced form factors; i.e., the contribution from the top-bottom loop and those from the Higgs-boson loop. The values of $F^{(t-b \text{ loop})}$ are given by $F^{(t-b \text{ loop})} \simeq 0.01 \cot \beta$; i.e., $|F^{(t-b \text{ loop})}|^2 \simeq 10^{-3}, 10^{-4}$ and 10^{-5} for $\tan \beta = 0.3, 1$ and 3 , respectively, where $\tan \beta$ is the ratio of vacuum expectation values for neutral components of the two Higgs doublets. The contribution of the Higgs boson loop can be important for $\tan \beta \gtrsim 3$, where the top-bottom loop contribution becomes suppressed because of the smaller Yukawa couplings[25]. The Higgs loop effect on F is constrained from perturbative unitarity[29, 30] as $|F^{(\text{bosonic loop})}|^2 \lesssim 10^{-5}$ for $3 \lesssim \tan \beta \lesssim 10$. Therefore, the value of $|F^{(2\text{HDM})}|^2$ can be at most $\sim 10^{-3}, 10^{-4}$ and 10^{-5} for $\tan \beta = 0.3, 1$ and $3 - 10$, respectively. In the MSSM, the loop effect of super partner particles can enhance the vertex especially in the moderate values of $\tan \beta$. However, its magnitude is not large and at most less than 10^{-5} [28] for $\tan \beta \gtrsim 3$.

In models with triplets, the $H^\pm W^\mp Z^0$ vertex generally appears at the tree level. A common feature of the tree level contribution to the form factor F is the fact that it is proportional to the vacuum expectation values (VEVs) of the triplet field[7, 12], $F \propto v'/v$, where v and v' represent the VEVs of the doublet and the triplet in the model, respectively. When more than one triplet appear in the model, v' should be taken as the combination of the VEVs for them. In the Littlest Higgs model, an additional complex triplet field appears in the effective theory. The electroweak data indicate $1 \lesssim v' \lesssim 4 \text{ GeV}$ for $f = 2 \text{ TeV}$ [31].

² We consider Model II 2HDM[7].

We here consider the case with $m_h = 115$ GeV, $f = 1$ TeV (2 TeV), $v' = 5$ GeV (4 GeV), and $m_{H^\pm} = 700$ GeV (1.56 TeV) as a reference: i.e., the value of the form factor F is $|F^{(\text{LLH})}|^2 \simeq 0.0085$ (0.0054).

In the model with additional real and complex triplet fields, the rho parameter can be set to be unity at the tree level, by imposing the custodial symmetry; i.e., $v'_r = v'_c (= v')$, where v'_r and v'_c are respectively the VEVs of the real and the complex triplet field[12, 13, 14]. The strongest experimental bound on v'/v comes from the $Zb\bar{b}$ result. The limits at 95% CL are $\tan\theta_H \lesssim 0.5, 1$ and 1.7 for the mass of the three-plet field of $SU(2)_V$ which do not couple to W^\pm and Z^0 to be 0.1, 0.5 and 1 TeV, respectively[15], where $\sin\theta_H = \sqrt{8v'^2/(v^2 + 8v'^2)}$. These limits imply $|F^{(\text{triplet})}|^2 = 0.26 - 0.97$.

III. SIGNAL AND BACKGROUNDS

A. Charged Higgs production via vector boson fusion

VBF is a pure electroweak process without color flow in the central region. The process naturally leads to high transverse momentum (P_T) tag jets in the forward region and allow to observe small hadronic activity in the central region except for jets from produced Higgs boson. Hence it is possible to observe small electroweak signal rates in a region of phase space not very populated by QCD background events. Such an advantage of VBF has been used for neutral Higgs boson production for intermediate and greater masses of Higgs bosons [1, 21, 22, 23, 24]. This can also be applied for charged Higgs boson production from WZ fusion, which we discuss in this paper.

In Fig. 1, the hadronic cross section of $pp \rightarrow W^\pm Z^0 X \rightarrow H^\pm X$ at the LHC ($\sqrt{s} = 14$ TeV) is shown as a function of mass m_{H^\pm} of the charged Higgs boson [20]. The form factors F , G and H of the $H^\pm W^\mp Z^0$ vertex are set to be 1, 0 and 0, respectively. The magnitude of $\sigma^{|F|^2=1}$ can be about 3900 fb for $m_{H^\pm} = 200$ GeV, 470 fb for $m_{H^\pm} = 500$ GeV, 210 fb for $m_{H^\pm} = 700$ GeV and 150 fb for $m_{H^\pm} = 800$ GeV. The prediction of the cross section in each new physics scenario can be obtained by rescaling the value of F . The typical values of F in several models are summarized in Sec. II.

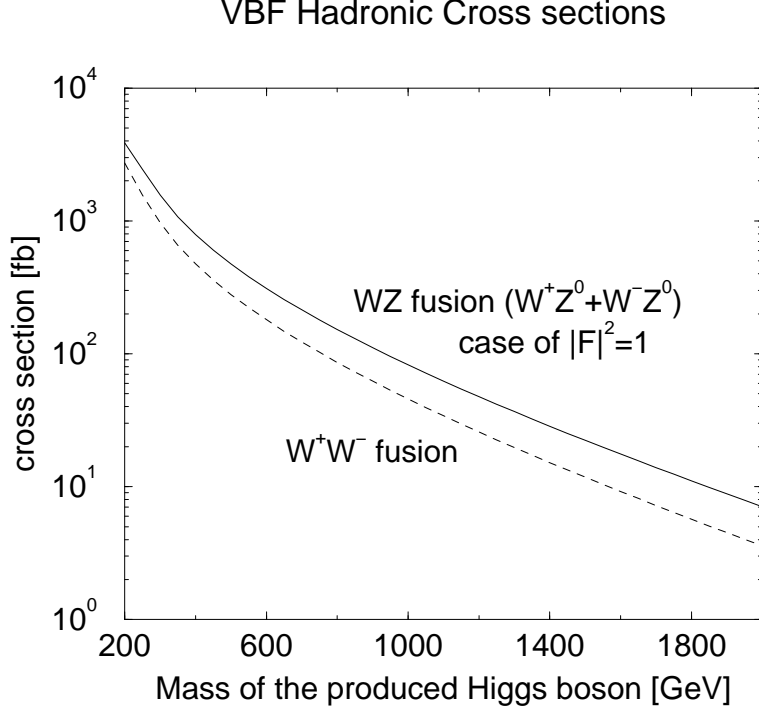


FIG. 1: The hadronic cross section of the $W^\pm Z^0$ fusion process and the W^+W^- fusion process as a function of the mass of the charged and neutral Higgs bosons, respectively. For the $W^\pm Z^0$ fusion, the form factor F is set to be unity. The SM prediction is shown for the W^+W^- fusion.

B. Event selection

1. Higgs production via VBF

Forward jet tagging

A characteristic of VBF is that the colliding quarks are scattered with relatively high P_T . These scattered partons can easily be identified as jets in forward region of the detector. Since the two forward jets j_1 and j_2 lie in opposite hemispheres with large pseudo-rapidity separation between them, we can impose the cut

$$\Delta\eta_{j_1 j_2} \equiv |\eta_{j_1} - \eta_{j_2}| > 2 - 4, \quad (3)$$

where the cut value is adjusted depending on the Higgs mass and decay modes so as to make it most effectively. With this cut, QCD backgrounds are typically suppressed by a few orders of magnitude, while the signal rate is suppressed at most by a factor of 2–3. We also impose the constraints for the invariant mass of two forward jets, whose physical meaning

is similar to that in the constraint in Eq. (3);

$$M_{j_1 j_2} > 500 - 1000 \text{ GeV}. \quad (4)$$

Central jet veto

Since VBF is a pure electroweak process without color flow in the central region, it allows us to observe small hadronic activity except for jets which are the tagging jets and the decay products from produced Higgs boson. We then impose the veto on the additional production of jets in the central region (between two tagging jets).

2. Higgs decay part

Here we consider the kinematic cuts for the $H^\pm \rightarrow t\bar{b}(\bar{t}b)$ and the $H^\pm \rightarrow W^\pm Z^0$ processes, separately. We impose the basic cuts for the invariant mass, and those for the number of jets, b -jets and leptons which should be the appropriate number for each final state. In order to improve the significance S/\sqrt{B} , we impose further several effective cuts which we explain below.

The $H^\pm \rightarrow t\bar{b}(\bar{t}b)$ mode

The final state $2b + \ell + \cancel{E}_T$ with two tagging jets is studied here. The main background is the top pair production whose cross section amounts to about 490 pb.

For the $H^- \rightarrow \bar{t}b$ mode, one b -jet (b) comes directly from the H^- decay, and the other b -jet (\bar{b}) does from the decay of the top quark which is a decay product of H^- . For H^- with a relatively large mass, the former b -jet tends to have higher P_T than the b -jet from the top quark decay. Then, the cut for the b -jet with higher P_T is helpful for reducing the top pair production events. The same happens for the $H^+ \rightarrow t\bar{b}$ mode (Fig. 2).

The $H^\pm \rightarrow W^\pm Z^0$ mode

For the model with a real and a complex triplet fields [12, 13, 14], the $H^\pm \rightarrow W^\pm Z^0$ decay mode is dominant because H^\pm do not couple to fermions. We consider the sequential decay mode $W^\pm \rightarrow \ell^\pm \nu$ and $Z \rightarrow jj$ or $\ell\ell$, that is, the final states are the $2j + \ell + \cancel{E}_T$ and $3\ell + \cancel{E}_T$ with two tagging jets. For the $jj\ell\nu$ mode, the most serious background comes from the $W + 4jets$ events. Even after the forward jet tagging ($\Delta\eta_{j_1 j_2} > 2.5$ and $M_{j_1 j_2} > 500$

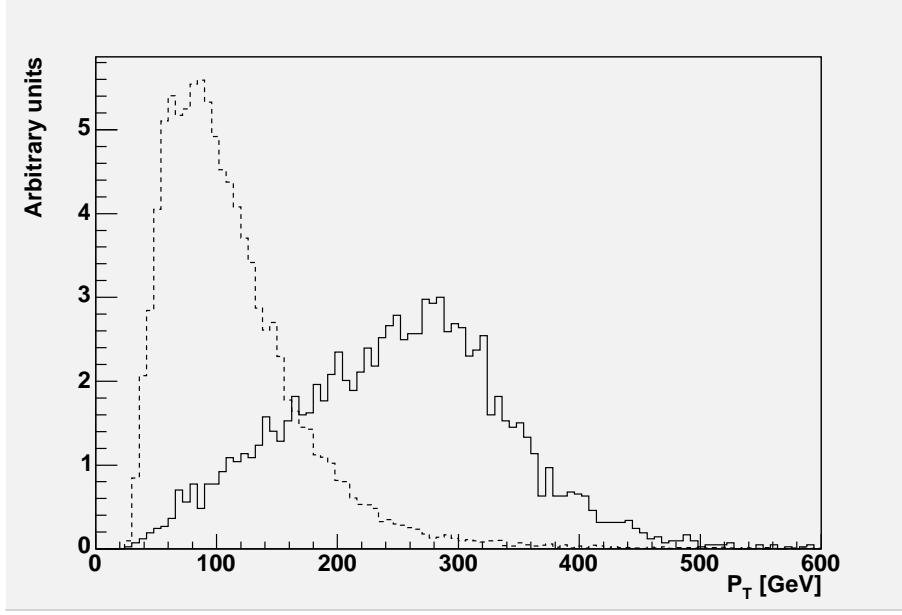


FIG. 2: The P_T distribution for the b -jets with the highest P_T from the signal ($pp \rightarrow W^\pm Z^0 X \rightarrow H^\pm X \rightarrow tbX$ at $m_H^\pm = 700$ GeV) and background (top pair production). Solid (dashed) histogram represents the signal (top pair production).

GeV), the cross section exceeds 130 pb. Though the top pair production is also the serious background, eliminating the events which have two b -jets drastically reduces the background from the top pair production [23].

Since the $W + 4jets$ events are dominated by single W boson production processes $u\bar{d}(\bar{u}d) \rightarrow W^\pm$ at the parton level, the helicities of the produced W bosons do not have the helicity 0 component. Then, the leptons coming from the W bosons are populated in the forward and backward direction, according to $|\mathcal{M}(W^\pm \rightarrow \ell^\pm \nu)|^2 \sim |1 \pm \cos \theta|^2$ where θ is the scattering angle in the center-of-mass frame. On the other hand, W bosons coming from the H^\pm bosons are not polarized. Then, if we put a cut for the lepton direction, such as $\eta_\ell < 1$ where η_ℓ is the pseudo-rapidity of the lepton, a large amount of backgrounds can be effectively reduced (Fig. 3).

When H^\pm has relatively large masses, the produced W and Z bosons have large momenta and the trajectories of their decay products follow directions of their parent W and Z bosons approximately. Therefore, if the jets in the central region are labeled as j_3 and j_4 , and if the quantities $\Delta R_{min} = \min(\Delta R_{\ell j_3}, \Delta R_{\ell j_4})$ and $\Delta R_{max} = \max(\Delta R_{\ell j_3}, \Delta R_{\ell j_4})$ are defined, where $\Delta R \equiv \sqrt{|\Delta\phi|^2 + |\Delta\eta|^2}$, the relation $\Delta R_{min} \simeq \Delta R_{max}$ is obtained for the signal

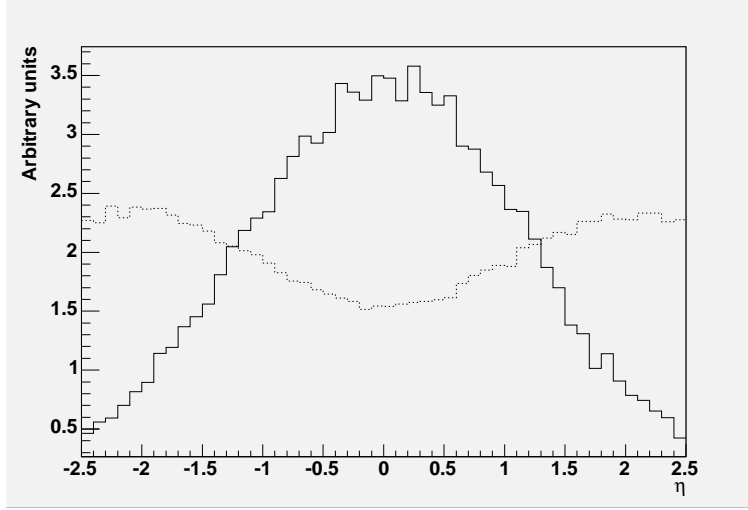


FIG. 3: The distribution for the pseudo-rapidity η of electrons from the signal ($pp \rightarrow W^\pm Z^0 X \rightarrow H^\pm X \rightarrow W^\pm Z^0 X \rightarrow jj\ell\nu X$ at $m_H^\pm = 800$ GeV) and backgrounds (top pair production, $W + 4j$). Solid (dotted) histogram represents the signal ($W + 4j$).

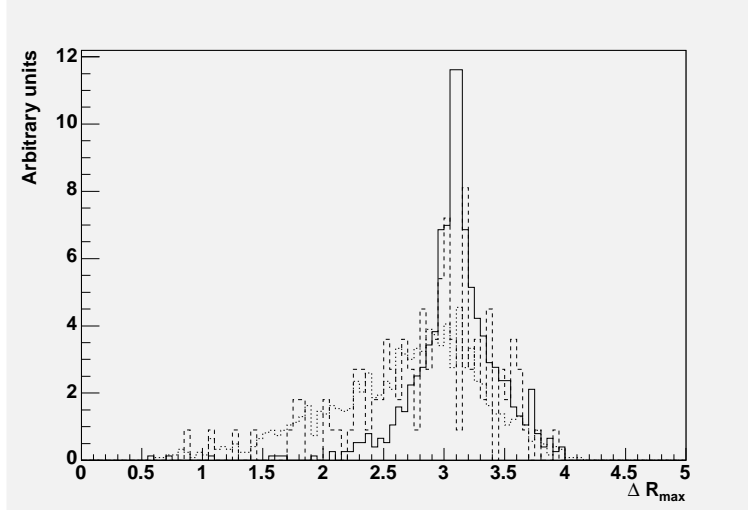


FIG. 4: The distribution for ΔR_{max} from the signal ($pp \rightarrow W^\pm Z^0 X \rightarrow H^\pm X \rightarrow W^\pm Z^0 X \rightarrow jj\ell\nu X$ at $m_H^\pm = 800$ GeV) and backgrounds (top pair production, $W + 4j$). Solid (dashed, dotted) histogram represents the signal (top pair production, $W + 4j$).

process. On the other hand, the background processes do not necessarily satisfy this relation (Fig. 4 and Fig. 5). In addition, the jet-jet separation $\Delta R_{j_3 j_4}$ has small value for the signal process (Fig. 6), so that we impose the cut $\Delta R_{j_3 j_4} < 1$.

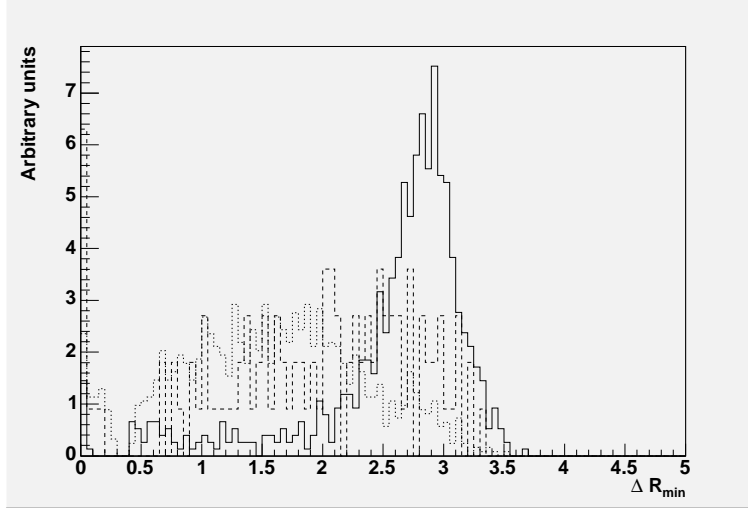


FIG. 5: The distribution for ΔR_{\min} from the signal ($pp \rightarrow W^\pm Z^0 X \rightarrow H^\pm X \rightarrow W^\pm Z^0 X \rightarrow jj\ell\nu X$ at $m_H^\pm = 800$ GeV) and backgrounds (top pair production, $W + 4j$). Solid (dashed, dotted) histogram represents the signal (top pair production, $W + 4j$).

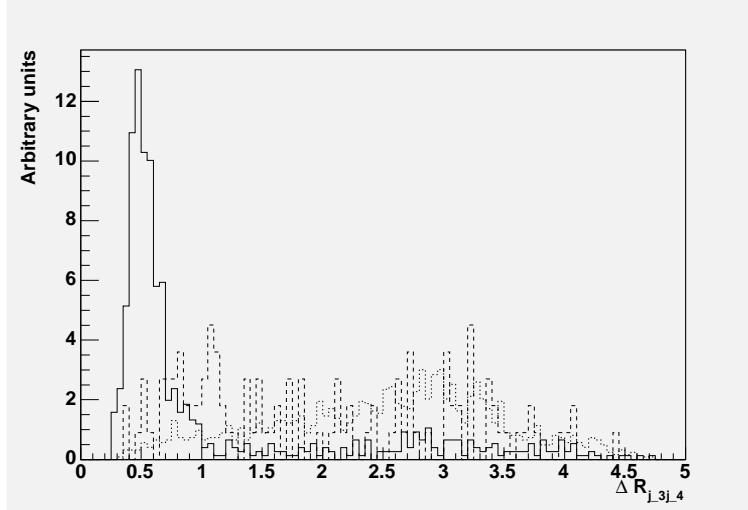


FIG. 6: The distribution for ΔR_{j3j4} from the signal ($pp \rightarrow W^\pm Z^0 X \rightarrow H^\pm X \rightarrow W^\pm Z^0 X \rightarrow jj\ell\nu X$ at $m_H^\pm = 800$ GeV) and backgrounds (top pair production, $W + 4j$). Solid (dashed, dotted) histogram represents the signal (top pair production, $W + 4j$).

C. Results

The event generation for the processes except for $W^\pm Z^0 jj$ production is performed by PYTHIA 6.2 [32].³ We use the CTEQ5L parametrization [33] of the parton distribution functions. For the $W^\pm Z^0 jj$ production, we use MadGraph [34] where the CTEQ6L [35] is adopted. In our study, we assume the branching ratio of the charged Higgs decay into each mode ($H^\pm \rightarrow t\bar{b}$ ($\bar{t}b$) and $H^\pm \rightarrow W^\pm Z^0$) is 100% in order to give results in a model-independent way. When a particular model is considered, we have to multiply the branching ratios properly. For the detector performance we applied acceptance cuts and included smearing effects according to the ATLAS detector[36]. For $W + 4j$ events, the events with $M_{j_1 j_2} > 500$ GeV and $\Delta\eta_{j_1 j_2} > 2.5$ are used in our simulation study.

$$1. \quad pp \rightarrow W^\pm Z^0 X \rightarrow H^\pm X \rightarrow tbX$$

$$\underline{H^\pm \rightarrow t\bar{b} \ (\bar{t}b) \rightarrow bbl\nu}$$

The results of the efficiency for selection cuts are listed in Table I and II for $m_{H^\pm} = 200$ and 700 GeV, respectively. The cuts applied in this analysis are:

- Forward jet tagging:

At least one jet in both forward ($\eta \geq 0$) and backward ($\eta < 0$) regions with $P_T > 25$ GeV.

By defining a jet with the highest P_T in the forward (backward) region as j_1 (j_2),

$$\Delta\eta_{j_1 j_2} > 3.8, M_{j_1 j_2} > 550 \text{ GeV for } m_{H^\pm} = 200 \text{ GeV,}$$

$$\Delta\eta_{j_1 j_2} > 3.5, M_{j_1 j_2} > 800 \text{ GeV for } m_{H^\pm} = 700 \text{ GeV.}$$

- Lepton cuts:

One lepton with $P_T > 30$ GeV.

- b -jet cuts:

Two b -jets with $P_T > 25$ GeV.

(P_T of one b -jet with higher P_T) > 250 GeV for $m_{H^\pm} = 700$ GeV.

³ We use the neutral Higgs boson production process via VBF as a signal process. In order to deal with the process of charged Higgs boson production we compel the produced neutral Higgs bosons to decay into $t\bar{b}$ ($\bar{t}b$) or $W^\pm Z^0$ in the generation.

	signal	background $t\bar{t}$
Before cuts	100% (170 fb)	100% (490 pb)
+Forward jet tagging	29% (49 fb)	4.1% (20 pb)
+Lepton cuts	4.1% (7.0 fb)	0.81% (4.0 pb)
+ b -jet cuts	1.0% (1.7 fb)	0.42% (2.1 pb)
+Central jet veto	0.66% (1.1 fb)	0.060% (0.29 pb)
+invariant mass cuts	0.32% (0.54 fb)	0.0036% (18 fb)

TABLE I: Efficiencies and cross sections for the signal ($pp \rightarrow W^\pm Z^0 X \rightarrow H^\pm X \rightarrow tbX \rightarrow bbl\nu X$ at $m_{H^\pm} = 200$ GeV) and the background (top pair production). The cross sections are shown in parenthesis. For the signal, we show the cross sections which give $S/\sqrt{B} \simeq 3$ for $|F|^2 = 1$.

- Central jet veto:

No jet with $P_T > 20$ GeV and $\Delta R > 0.7$ from tag jets.

- invariant mass cuts:

$M_{bbl\nu} < 220$ GeV for $m_{H^\pm} = 200$ GeV.

	signal	background $t\bar{t}$
Before cuts	100% (23 fb)	100% (490 pb)
+Forward jet tagging	32% (7.4 fb)	2.1% (10.0 pb)
+Lepton cuts	5.5% (1.3 fb)	0.42% (2.1 pb)
+ b -jet cuts	2.1% (0.48 fb)	0.0065% (0.032 pb)
+Central jet veto	1.1% (0.25 fb)	0.00079% (3.9 fb)

TABLE II: Efficiencies and cross sections for the signal ($pp \rightarrow W^\pm Z^0 X \rightarrow H^\pm X \rightarrow tbX \rightarrow bbl\nu X$ at $m_{H^\pm} = 700$ GeV) and the background (top pair production) for $H^\pm \rightarrow t\bar{b}(\bar{t}b)$ decay mode. The cross sections are shown in parenthesis. For the signal, we show the cross sections which give $S/\sqrt{B} \simeq 3$ for $|F|^2 = 1$.

After these cuts are imposed, the signal events decrease to 0.32% (1.1%) for $m_{H^\pm} = 200$ GeV (700 GeV), while a large reduction by about 2 orders (3 orders) of magnitude is observed in the background processes. Since the cross section for the top pair production is 490 pb, the signal cross sections of 170 fb and 23 fb are required to satisfy the statistical significance $S/\sqrt{B} > 3$ for $m_{H^\pm} = 200$ and 700 GeV, respectively, assuming the integrated luminosity as $\mathcal{L} = 600 \text{ fb}^{-1}$ and the lepton detection efficiency as 90%.

$$2. \quad pp \rightarrow W^\pm Z^0 X \rightarrow H^\pm X \rightarrow W^\pm Z^0 X$$

$$\underline{H^\pm \rightarrow W^\pm Z^0 \rightarrow jj\ell\nu}$$

Efficiencies for the selection cuts are listed in Table III, IV and V for $m_{H^\pm} = 200, 500$ and 800 GeV, respectively. The cuts applied in this analysis are:

- Forward jet tagging:

At least one jet in both forward ($\eta \geq 0$) and backward ($\eta < 0$) regions with $P_T > 40$ GeV.

By defining a jet with the highest P_T in the forward (backward) region as j_1 (j_2),
 $\Delta\eta_{j_1 j_2} > 2.5$, $M_{j_1 j_2} > 500$ GeV.

- b -jet cuts:

No b -jet with $P_T > 25$ GeV.

- Lepton cuts:

One lepton with $P_T > 30$ GeV and no other lepton with $P_T > 20$ GeV,

$(M_{\ell\nu})_T < 100$ GeV,

$\eta_\ell < 1.0$.

- Central jet veto:

Two jets with $P_T > 20$ GeV in the central region ($\eta < 2.0$).

- Central jet cuts:

$(P_T \text{ of one central jet with higher } P_T) > 50$ GeV for $m_{H^\pm} = 200$ GeV,

$(P_T \text{ of one central jet with higher } P_T) > 100$ GeV for $m_{H^\pm} = 500, 800$ GeV,

$\Delta R_{j_3 j_4} < 1.0$ and $\Delta R_{max} > 2.5$ for $m_{H^\pm} = 500$ GeV,

$\Delta R_{j_3 j_4} < 1.0$, $\Delta R_{min} > 2.5$ for $m_{H^\pm} = 800$ GeV,
 $60 \text{ GeV} < M_{j_3 j_4} < 100 \text{ GeV}$.

	signal	backgrounds	
		$W + 4j$	$t\bar{t}$
Before cuts	100% (910 fb)	100% (130 pb)	100% (490 pb)
+Forward jet tagging	31% (280 fb)	50% (65 pb)	3.6% (18 pb)
+ b -jet cuts	26% (240 fb)	47% (61 pb)	0.25% (1.2 pb)
+Lepton cuts	1.3% (12 fb)	2.0% (2.6 pb)	0.012% (0.059 pb)
+Central jet veto	0.39% (3.5 fb)	0.32% (0.42 pb)	0.0033% (0.016 pb)
+Central jet cuts	0.11% (1.0 fb)	0.043% (56 fb)	0.00079% (3.9 fb)
	backgrounds		
	$W^+ Z^0 jj$	$W^- Z^0 jj$	WZ
Before cuts	100% (350 fb)	100% (210 fb)	100% (26 pb)
+Forward jet tagging	43% (150 fb)	36% (76 fb)	1.1% (0.29 pb)
+ b -jet cuts	37% (130 fb)	30% (63 fb)	0.99% (0.26 pb)
+Lepton cuts	1.5% (5.3 fb)	1.2% (2.5 fb)	0.015% (0.0039 pb)
+Central jet veto	0.40% (1.4 fb)	0.30% (0.63 fb)	0.0031% (0.81 fb)
+Central jet cuts	0.081% (0.28 fb)	0.072% (0.15 fb)	0.0006% (0.16 fb)

TABLE III: Efficiencies and cross sections for the signal ($pp \rightarrow W^\pm Z^0 X \rightarrow H^\pm X \rightarrow W^\pm Z^0 X \rightarrow jj\ell\nu X$ at $m_H^\pm = 200$ GeV) and backgrounds ($W + 4j$, top pair production, $W^+ Z^0 jj$, $W^- Z^0 jj$, WZ production). The cross sections are shown in parenthesis. For the signal, we show the cross sections which give $S/\sqrt{B} \simeq 3$ for $|F|^2 = 1$.

The event selection also works effectively in order to reduce the WZ production whose cross section is 26 pb. According to our simulation study, the number of remaining events for the WZ and $WZjj$ production processes is less than the one for $W + 4jet$ production by at least 2 orders.

Since the cross section for the $W + 4jet$ production (the top pair production) is about 130 pb (490 pb), the signal cross sections of 910 fb, 140 fb and 51 fb are required to satisfy

	signal	backgrounds	
		$W + 4j$	$t\bar{t}$
Before cuts	100% (140 fb)	100% (130 pb)	100% (490 pb)
+Forward jet tagging	40% (56 fb)	50% (65 pb)	3.6% (18 pb)
+ b -jet cuts	33% (46 fb)	47% (61 pb)	0.25% (1.2 pb)
+Lepton cuts	2.0% (2.8 fb)	2.0% (2.6 pb)	0.012% (0.059 pb)
+Central jet veto	0.62% (0.87 fb)	0.32% (0.42 pb)	0.0033% (0.016 pb)
+Central jet cuts	0.19% (0.27 fb)	0.0027% (3.5 fb)	0.0001% (0.49 fb)

	backgrounds		
	$W^+ Z^0 jj$	$W^- Z^0 jj$	WZ
Before cuts	100% (350 fb)	100% (210 fb)	100% (26 pb)
+Forward jet tagging	43% (150 fb)	36% (76 fb)	1.1% (0.29 pb)
+ b -jet cuts	37% (130 fb)	30% (63 fb)	0.99% (0.26 pb)
+Lepton cuts	1.5% (5.3 fb)	1.2% (2.5 fb)	0.015% (0.0039 pb)
+Central jet veto	0.40% (1.4 fb)	0.30% (0.63 fb)	0.0031% (0.81 fb)
+Central jet cuts	0.018% (0.063 fb)	0.022% (0.046 fb)	0.0001% (0.026 fb)

TABLE IV: Efficiencies and backgrounds for the signal ($pp \rightarrow W^\pm Z^0 X \rightarrow H^\pm X \rightarrow W^\pm Z^0 X \rightarrow jj\ell\nu X$ at $m_H^\pm = 500$ GeV) and backgrounds ($W + 4j$, top pair production, $W^+ Z^0 jj$, $W^- Z^0 jj$, WZ production). The cross sections are shown in parenthesis. For the signal, we show the cross sections which give $S/\sqrt{B} \simeq 3$ with $|F|^2 = 1$.

$S/\sqrt{B} > 3$ for $m_{H^\pm} = 200, 500$ and 800 GeV, respectively, under $\mathcal{L} = 600 \text{ fb}^{-1}$ and the 90% lepton detection efficiency.

$$\underline{H^\pm \rightarrow W^\pm Z^0 \rightarrow \ell\ell\ell\nu}$$

Efficiencies for the selection cuts are listed in Table VI, VII and VIII for $m_{H^\pm} = 200, 500$ and 800 GeV, respectively. The cuts applied in this analysis are:

- Forward jet tagging:

At least one jet in both forward ($\eta \geq 0$) and backward ($\eta < 0$) regions with $P_T > 40$ GeV.

	signal		backgrounds	
			$W + 4j$	$t\bar{t}$
Before cuts	100%	(51 fb)	100% (130 pb)	100% (490 pb)
+Forward jet tagging	46%	(23 fb)	50% (65 pb)	3.6% (18 pb)
+ b -jet cuts	38%	(19 fb)	47% (61 pb)	0.25% (1.2 pb)
+Lepton cuts	2.5%	(1.3 fb)	2.0% (2.6 pb)	0.012% (0.059 pb)
+Central jet veto	0.88%	(0.45 fb)	0.32% (0.42 pb)	0.0033% (0.016 pb)
+Central jet cuts	0.42%	(0.21 fb)	0.0016% (2.1 fb)	0.0001% (0.49 fb)

	backgrounds		
	$W^+ Z^0 jj$	$W^- Z^0 jj$	WZ
Before cuts	100% (350 fb)	100% (210 fb)	100% (26 pb)
+Forward jet tagging	43% (150 fb)	36% (76 fb)	1.1% (0.29 pb)
+ b -jet cuts	37% (130 fb)	30% (63 fb)	0.99% (0.26 pb)
+Lepton cuts	1.5% (5.3 fb)	1.2% (2.5 fb)	0.015% (0.0039 pb)
+Central jet veto	0.40% (1.4 fb)	0.30% (0.63 fb)	0.0031% (0.81 fb)
+Central jet cuts	0.014% (0.049 fb)	0.018% (0.038 fb)	0.0001% (0.026 fb)

TABLE V: Efficiencies and backgrounds for the signal ($pp \rightarrow W^\pm Z^0 X \rightarrow H^\pm X \rightarrow W^\pm Z^0 X \rightarrow jj\ell\nu X$ at $m_H^\pm = 800$ GeV) and backgrounds ($W + 4j$, top pair production, $W^+ Z^0 jj$, $W^- Z^0 jj$, WZ production) for . The cross sections are shown in parenthesis. For the signal, we show the cross sections which give $S/\sqrt{B} \simeq 3$ for $|F|^2 = 1$.

By defining a jet with the highest P_T in the forward (backward) region as j_1 (j_2),
 $\Delta\eta_{j_1 j_2} > 2.5$, $M_{j_1 j_2} > 500$ GeV.

- Lepton cuts:

Three leptons with $P_T > 30$ GeV and no other lepton with $P_T > 20$ GeV.

By defining two leptons whose combination minimizes the quantity $M_{\ell_i \ell_j} - m_Z$ ($i, j = 1 - 3$, m_Z is the mass of the Z boson.) as ℓ_{Z_1} and ℓ_{Z_2} ,

$$\Delta R_{\ell_{Z_1} \ell_{Z_2}} < 1.0 \text{ for } m_{H^\pm} = 800 \text{ GeV},$$

$$80 \text{ GeV} < M_{\ell_{Z_1} \ell_{Z_2}} < 100 \text{ GeV},$$

	signal		backgrounds			
			W^+Z^0jj	W^-Z^0jj	WZ	
Before cuts	100%	(210 fb)	100% (350 fb)	100% (210 fb)	100%	(26 pb)
+Forward jet tagging	31%	(65 fb)	43% (150 fb)	36% (76 fb)	1.1%	(0.29 pb)
+Lepton cuts	0.017%	(0.036 fb)	0.0040% (0.014 fb)	0.0040% (0.0084 fb)	(< 0.0026 fb)	

TABLE VI: Efficiencies and cross sections for the signal ($pp \rightarrow W^\pm Z^0 X \rightarrow H^\pm X \rightarrow W^\pm Z^0 X \rightarrow \ell\ell\ell\nu X$ at $m_H^\pm = 200$ GeV) and backgrounds (W^+Z^0jj , W^-Z^0jj , WZ production). The cross sections are shown in parenthesis. For the signal, we show the cross sections which give $S/\sqrt{S+B} \simeq 3$ for $|F|^2 = 1$.

	signal		backgrounds			
			W^+Z^0jj	W^-Z^0jj	WZ	
Before cuts	100%	(110 fb)	100% (350 fb)	100% (210 fb)	100%	(26 pb)
+Forward jet tagging	40%	(44 fb)	43% (150 fb)	36% (76 fb)	1.1%	(0.29 pb)
+Lepton cuts	0.030%	(0.033 fb)	0.0040% (0.014 fb)	(< 0.0042 fb)	(< 0.0026 fb)	

TABLE VII: Efficiencies and cross sections for the signal ($pp \rightarrow W^\pm Z^0 X \rightarrow H^\pm X \rightarrow W^\pm Z^0 X \rightarrow \ell\ell\ell\nu X$ at $m_H^\pm = 500$ GeV) and backgrounds (W^+Z^0jj , W^-Z^0jj , WZ production). The cross sections are shown in parenthesis. For the signal, we show the cross sections which give $S/\sqrt{S+B} \simeq 3$ for $|F|^2 = 1$.

$$170 \text{ GeV} < M_{\ell\ell\ell\nu} < 240 \text{ GeV for } m_{H^\pm} = 200 \text{ GeV},$$

$$450 \text{ GeV} < M_{\ell\ell\ell\nu} < 600 \text{ GeV for } m_{H^\pm} = 500 \text{ GeV}.$$

Since the cross section for the W^+Z^0jj production (the W^-Z^0jj production) is about 350 fb (210 fb), the signal cross sections of 210 fb, 110 fb and 67 fb are required to satisfy $S/\sqrt{S+B} > 3$ for $m_{H^\pm} = 200, 500$ and 800 GeV, respectively, under $\mathcal{L} = 600 \text{ fb}^{-1}$ and the 90% lepton detection efficiency.

	signal		backgrounds			
			W^+Z^0jj	W^-Z^0jj	WZ	
Before cuts	100%	(67 fb)	100% (350 fb)	100% (210 fb)	100%	(26 pb)
+Forward jet tagging	46%	(31 fb)	43% (150 fb)	36% (76 fb)	1.1%	(0.29 pb)
+Lepton cuts	0.090%	(0.060 fb)	0.026% (0.091 fb)	0.010% (0.021 fb)		(< 0.0026 fb)

TABLE VIII: Efficiencies and cross sections for the signal ($pp \rightarrow W^\pm Z^0 X \rightarrow H^\pm X \rightarrow W^\pm Z^0 X \rightarrow \ell\ell\ell\nu X$ at $m_H^\pm = 800$ GeV) and backgrounds (W^+Z^0jj , W^-Z^0jj , WZ production). The cross sections are shown in parenthesis. For the signal, we show the cross sections which give $S/\sqrt{S+B} \simeq 3$ for $|F|^2 = 1$.

IV. DISCUSSIONS

A. $pp \rightarrow W^\pm Z^0 X \rightarrow H^\pm X \rightarrow tbX$

In the 2HDM and the MSSM, although there are potentially many decay modes, the main mode would be the decay into a tb pair as long as it is kinematically allowed. The main decay mode of the Littlest Higgs model would also be the decay into a tb pair [10]. In these cases, the signal can be a $b\bar{b}\ell\nu$ ($\ell = e$ and μ) event. As shown in Sec. III, the required cross section to satisfy $S/\sqrt{B} \gtrsim 3$ after background reduction is $\sigma_S \gtrsim 170$ fb (23 fb) for $m_{H^\pm} = 200$ GeV (700 GeV), which corresponds to $|F|^2 \gtrsim 0.044$ ($|F|^2 \gtrsim 0.11$), where σ_S is the signal cross section before kinematical cuts. Hence, the typical values of $|F|^2$ in the 2HDM, the MSSM and the Littlest Higgs model are all smaller than the required one for $S/\sqrt{B} \gtrsim 3$ ⁴. Therefore, we must conclude that testing these models through this process is challenging.

B. $pp \rightarrow W^\pm Z^0 X \rightarrow H^\pm X \rightarrow W^\pm Z^0 X$

In models with triplets that do not couple to fermions, it would mainly decay into a WZ pair. The model with a real and a complex triplets can correspond to this case. The signal

⁴ When the variation of the models such as the Littlest Higgs model with only gauging the SM $U(1)_Y$ subgroup [37] are considered, the F values can be larger. Then, the observation may be possible.

m_H^\pm (GeV)	200	700
$ F ^2$ for $bbl\nu$	0.044	0.11

TABLE IX: Required $|F|^2$ values for $S/\sqrt{B} \sim 3$ for the $pp \rightarrow W^\pm Z^0 X \rightarrow H^\pm X \rightarrow tbX \rightarrow bbl\nu$ mode at $\mathcal{L} = 600 \text{ fb}^{-1}$.

m_H^\pm (GeV)	200	500	800
$ F ^2$ for $jjl\nu$	0.23	0.30	0.34
$ F ^2$ for $\ell\ell\nu$	0.054	0.23	0.45

TABLE X: Required $|F|^2$ values for $S/\sqrt{B} \sim 3$ for the $pp \rightarrow W^\pm Z^0 X \rightarrow H^\pm X \rightarrow W^\pm Z^0 X \rightarrow jjl\nu X$ and $\ell\ell\nu X$ modes at $\mathcal{L} = 600 \text{ fb}^{-1}$.

event can be $jjl\nu$ and $\ell\ell\nu$.

For the $jjl\nu$ event, the required values of the production cross section to satisfy the statistical significance $S/\sqrt{B} \gtrsim 3$ after background reduction is $\sigma_S \gtrsim 910, 140$ and 51 fb for $m_{H^\pm} = 200, 500$ and 800 GeV , respectively. The corresponding values of $|F|^2$ are $|F|^2 \gtrsim 0.23, 0.30$ and 0.34 . For the $\ell\ell\nu$ event, the required values of the production cross section to satisfy the statistical significance $S/\sqrt{S+B} \gtrsim 3$ after background reduction is $\sigma_S \gtrsim 210, 110$ and 67 fb for $m_{H^\pm} = 200, 500$ and 800 GeV , respectively. The corresponding values of $|F|^2$ are $|F|^2 \gtrsim 0.054, 0.23$ and 0.45 . The results are similar to those in Ref. [38].

Therefore, this model can be tested via the process $pp \rightarrow W^\pm Z^0 X \rightarrow H^\pm X \rightarrow W^\pm Z^0 X$.

V. CONCLUSIONS

The $H^\pm W^\mp Z^0$ vertex strongly depends on the structure of the Higgs sector in various new physics scenarios, so that its measurement can be useful to distinguish the models. In this paper, the possibility of measuring this vertex has been studied by using the single H^\pm production via WZ fusion at the LHC. A signal and background simulation under the expected detector performance at the LHC is performed. Required values of $|F|^2$ for $S/\sqrt{B} \gtrsim 3$ are obtained for the $pp \rightarrow W^\pm Z^0 X \rightarrow H^\pm X \rightarrow tbX \rightarrow bbl\nu X$ mode and the $pp \rightarrow W^\pm Z^0 X \rightarrow H^\pm X \rightarrow W^\pm Z^0 X \rightarrow jjl\nu X$ and $\ell\ell\nu X$ modes :see Tables IX and X,

respectively.

The process of $pp \rightarrow W^\pm Z^0 X \rightarrow H^\pm X \rightarrow tbX \rightarrow bbl\nu X$ can be used to test $H^\pm W^\mp Z^0$ vertex in multi-Higgs doublet models, the MSSM as well as the Littlest Higgs model. However, the required magnitude of the form factor F for the observation via WZ fusion at the LHC is turned out to be above the predicted maximal values of $|F|^2$ in these models. The maximal value of $|F|^2$ in the 2HDM is less by 2 orders than the required magnitude of $|F|^2$, and in the Littlest Higgs model the predicted $|F|^2$ values are less than the required $|F|^2$ value by 1 order. If we go to the SLHC, the 10 times larger luminosity may be expected. However, it is not easy to observe because the b tagging efficiency should be much worse than that of the LHC. Finally, although we have concentrated on WZ fusion in this paper, the $H^\pm W^\mp Z^0$ coupling may also be studied by using $gb \rightarrow H^\pm t \rightarrow W^\pm Z^0 t$ for models which include the sizable coupling of $H^\pm tb$ like in the 2HDM if the background can be greatly reduced.

On the other hand, it turns out that the process of $pp \rightarrow W^\pm Z^0 X \rightarrow H^\pm X \rightarrow W^\pm Z^0 X \rightarrow \ell\ell\nu X$ and $jj\ell\nu X$ can be useful to test the model with a real and a complex triplet fields.

Acknowledgments

The authors would like to thank Shoji Asai, Tomio Kobayashi and Mihoko Nojiri for useful discussions. A part of this work started in the discussion during the workshop “Physics in LHC era” at YITP, 13-15 December 2004 (YITP-W-04-20). S.K. was supported, in part, by Grants-in-Aid of the Ministry of Education, Culture, Sports, Science and Technology, Government of Japan, Grant Nos. 17043008 and 18034004.

-
- [1] ATLAS Collaboration, *Detector and Physics Performance Technical Design Report*, CERN/LHCC/99-14 (1999); CMS Collaboration, *CMS Technical proposal*, CERN/LHCC 94-38, CERN (1994).
 - [2] A.C. Bawa, C.S. Kim and A.D. Martin, Z. Phys. C 47 (1990) 75; L.G. Jin, et al., Eur. Phys. J. C 14 (2000) 91; A. Belyaev, et al., J. High Energy Phys. 06 (2002) 059; S.H. Zhu, hep-ph/0112109; T. Plehn, PRD 67 (2003) 014018; E.L. Berger, et al., hep-ph/0312286. M. Drees and D.P. Roy, Phys. Lett. B 269 (1991) 155; J.F. Gunion, Phys. Lett. B 322 (1994)

- 125; V.D. Barger, R.J. Phillips and D.P. Roy, Phys. Lett. B 324 (1994) 236; K. Odagiri, Phys. Lett. B 452 (1999) 327; S. Moretti and D.P. Roy, Phys. Lett. B 470 (1999) 209; D.P. Roy, Phys. Lett. B 277 (1992) 183 and Phys. Lett. B 459 (1999) 607; K.A. Assamagan, Y. Coadou and A. Deandrea, ATLAS note, SN-ATLAS-2002-017, hep-ph/0203121; R. Kinnunen, CMS NOTE 2000/045. K.A. Assamagan and N. Gollub, hep-ph/0406013.
- [3] S. Willenbrock, Phys. Rev. D 35 (1987) 173; O. Brein and W. Hollik, Eur. Phys. J. C 13 (2000) 175; A.A. Barrientos Bendezu and B.A. Kniehl, Phys. Rev. D 64 (2001) 035006.
- [4] D.A. Dicus, et al., Phys. Rev. D 40 (1989) 787; A.A. Barrientos Bendezu and B.A. Kniehl, Phys. Rev. D 59 (1999) 015009; S. Moretti and K. Odagiri, Phys. Rev. D 59 (1999) 055008; O. Brein, W. Hollik and S. Kanemura, Phys. Rev. D 63 (2001) 095001; W. Hollik and S.H. Zhu, Phys. Rev. D 65 (2002) 075015; E. Asakawa, O. Brein and S. Kanemura, Phys. Rev. D 72 (2005) 055017.
- [5] C. Biscarat and M. Dosil, ATLAS note, ATL-PHYS-2003-038.
- [6] J.A. Grifols, A. Méndez, Phys. Rev. D 22 (1980) 1725; A.A. Iogansen, N.G. Uraltsev, V.A. Khoze, Sov. J. Nucl. Phys. 36 1982 717.
- [7] J.F. Gunion, et al., *The Higgs Hunter's Guide*, Addison-Wesley, New York, 1990.
- [8] J.C. Pati, A. Salam, Phys. Rev. D 10 (1974) 275; R.N. Mohapatra, J.C. Pati, Phys. Rev. D 11 (1975) 2558; G. Senjanovic, R.N. Mohapatra, Phys. Rev. D 12 (1975) 1502.
- [9] N. Arkani-Hamed, et al., J. High Energy Phys. 07 (2002) 034.
- [10] T. Han, et al., Phys. Rev. D 67 (2003) 095004.
- [11] N. Arkani-Hamed, S. Dimopoulos, Phys. Rev. D 65 (2002) 052003; N. Arkani-Hamed, et al., Phys. Rev. D 61 (2000) 116003; E. Ma, U. Sarkar, Phys. Rev. Lett. 80 (1998) 5716.
- [12] P. Galison, Nucl. Phys. B 232 (1984) 26; H. Georgi, M. Machacek, Nucl. Phys. B 262 (1985) 463; R. Chivukura, H. Georgi, Phys. Lett. B 182 (1986) 181.
- [13] M. Chanowitz, M. Golden, Phys. Lett. B 165 (1985) 105.
- [14] J. Gunion, R. Vega, J. Wudka, Phys. Rev. D 42 (1990) 1673; Phys. Rev. D 43 (1991) 2322.
- [15] H. Haber, H. Logan, Phys. Rev. D 62 (2000) 015011.
- [16] T.G. Rizzo, Mod. Phys. Lett. A 4 (1989) 2757; A. Méndez, A. Pomarol, Nucl. Phys. B 349 (1991) 369; J.L. Díaz-Cruz, J. Hernández-Sánchez, J.J. Toscano, Phys. Lett. B 512 (2001) 339.
- [17] M. Capdequi Peyranère, H.E. Haber, P. Irulegui, Phys. Rev. D 44 (1991) 191.

- [18] S. Kanemura, Phys. Rev. D 61 (2000) 095001.
- [19] A. Arhrib, R. Benbrik, M. Chabab, hep-ph/0607182.
- [20] E. Asakawa, S. Kanemura, Phys. Lett. B 626 (2005) 111.
- [21] R.N. Cahn et al., Phys. Rev. D 35 (1987) 1626; V.D. Barger, T. Han, R.J.N. Phillips, Phys. Rev. D 37 (1988) 2005; R. Kleiss, W.J. Stirling, Phys. Lett. B 200 (1988) 193; U. Baur, E.W.N. Glover, Nucl. Phys. B 347 (1990) 12; U. Baur, E.W.N. Glover, Phys. Lett. B 252 (1990) 683; V. Barger et al., Phys. Rev. D 44 (1991) 1426.
- [22] D. Rainwater, D. Zeppenfeld, J. High Energy Phys. 12 (1997) 005; D. Rainwater, D. Zeppenfeld, K. Hagiwara, Phys. Rev. D 59 (1999) 014037; T. Plehn, D. Rainwater, D. Zeppenfeld, Phys. Rev. D 61 (2000) 093005; T. Plehn, D. Rainwater, D. Zeppenfeld, Phys. Rev. Lett. 88 (2002) 051801; N. Kauer et al., Phys. Lett. B 503 (2001) 113; T. Plehn, D. Rainwater, Phys. Lett. B 520 (2001) 108.
- [23] D. Rainwater and D. Zeppenfeld, Phys. Rev. D 60 (1999) 113004.
- [24] S. Asai, et al., Eur. Phys. J. C 32S2 (2004) 19.
- [25] S. Kanemura, Eur. Phys. J. C 17 (2000) 473.
- [26] S.-H. Zhu, hep-ph/9901221; A. Arhrib, et al., Nucl. Phys. B 581 (2000) 34.
- [27] S. Kanemura, S. Moretti, K. Odagiri, J. High Energy Phys. 02 (2001) 011.
- [28] H.E. Logan, S. Su, Phys. Rev. D 66 (2002) 035001; Phys. Rev. D 67 (2003) 017703.
- [29] B.W. Lee, C. Quigg, H.B. Thacker, Phys. Rev. D 16 (1977) 1519.
- [30] H. Hüffel, G. Pocsik, Z. Phys. C 8 (1981) 13; J. Maalampi, J. Sirkka, I. Vilja, Phys. Lett. B 265 (1991) 371; S. Kanemura, T. Kubota, E. Takasugi, Phys. Lett. B 313 (1993) 155; A. Akeroyd, A. Arhrib, E.-M. Naimi, Phys. Lett. B 490 (2000) 119; I.F. Ginzburg, I.P. Ivanov, hep-ph/0312374.
- [31] M.-C. Chen, S. Dawson, Phys. Rev. D 70 (2004) 015003.
- [32] T. Sjöstrand, Comp. Phys. Comm. 82 (1994).
- [33] H.L. Lai, et al., EPC 12 (2000) 375.
- [34] T. Stelzer, W.F. Long, Comp.Phys. Comm. 81, 357 (1994); F. Maltoni, T. Stelzer, J. High Energy Phys. 0302 (2003) 027.
- [35] S. Kretzer, et al., Phys. Rev. D 69 (2004) 114005.
- [36] E. Richter-Was, D. Froidevaux, L. Poggioli, *ATLFAST 2.0, a fast simulation package for ATLAS*, ATLAS internal note ATL-PHYS-98-131 (1998).

- [37] C. Csaki et al., Phys. Rev. D 68 (2003) 035009.
- [38] A. Birkedal, K. Matchev, M. Perelstein, Phys. Rev. Lett. 94 (2005) 191803.